Guidance in Kagome-like photonic crystal fibres I: analysis of an ideal fibre structure

Lei Chen, Greg J. Pearce, Timothy A. Birks, and David M. Bird*

Centre for Photonics and Photonic Materials, Department of Physics, University of Bath, Bath, BA2 7AY, UK

*d.bird@bath.ac.uk

Abstract: Propagation of light in a square-lattice hollow-core photonic crystal fibre is analysed as a model of guidance in a class of photonic crystal fibres that exhibit broad-band guidance without photonic bandgaps. A scalar governing equation is used and analytic solutions based on transfer matrices are developed for the full set of modes. It is found that an exponentially localised fundamental mode exists for a wide range of frequencies. These analytic solutions of an idealised structure will form the basis for analysis of guidance in a realistic structure in a following paper.

OCIS codes: (060.2280) Fiber design and fabrication; (060.2400) Fiber properties.

References and links

1. R. F. Cregan, B. J. Mangan, J. C. Knight, T. A. Birks, P. S. J. Russell, P. J. Roberts, and D. C. Allan, "Single-Mode Photonic Band Gap Guidance of Light in Air," Science **285**, 1537–1539 (1999).
2. P. Roberts, F. Couny, H. Sabert, B. Mangan, D. Williams, L. Farr, M. Mason, A. Tomlinson, T. Birks, J. Knight, and P. S. J. Russell, "Ultimate low loss of hollow-core photonic crystal fibres," Opt. Express **13**, 236–244 (2005).
3. D. G. Ouzounov, F. R. Ahmad, D. Mller, N. Venkataraman, M. T. Gallagher, M. G. Thomas, J. Silcox, K. W. Koch, and A. L. Gaeta, "Generation of Megawatt Optical Solitons in Hollow-Core Photonic Band-Gap Fibers," Science **301**, 1702–1704 (2003).
4. A. R. Bhagwat and A. L. Gaeta, "Nonlinear optics in hollow-core photonic bandgap fibers," Opt. Express **16**, 5035–5047 (2008).
5. F. Couny, F. Benabid, and P. S. Light, "Large-pitch kagome-structured hollow-core photonic crystal fiber," Opt. Lett. **31**, 3574–3576 (2006).
6. F. Couny, P. J. Roberts, T. A. Birks, and F. Benabid, "Square-lattice large-pitch hollow-core photonic crystal fiber," Opt. Express **16**, 20626–20636 (2008).
7. F. Couny, F. Benabid, P. J. Roberts, P. S. Light, and M. G. Raymer, "Generation and Photonic Guidance of Multi-Octave Optical-Frequency Combs," Science **318**, 1118–1121 (2007).
8. A. Argyros and J. Pla, "Hollow-core polymer fibres with a kagome lattice: potential for transmission in the infrared," Opt. Express **15**, 7713–7719 (2007).
9. G. J. Pearce, G. S. Wiederhecker, C. G. Poulton, S. Burger, and P. S. J. Russell, "Models for guidance in kagome-structured hollow-core photonic crystal fibres," Opt. Express **15**, 12680–12685 (2007).
10. S. Février, B. Beaudou, and P. Viale, "Understanding origin of loss in large pitch hollow-core photonic crystal fibers and their design simplification," Opt. Express **18**, 5142–5150 (2010).
11. A. W. Snyder and J. D. Love, *Optical Waveguide Theory* (Chapman & Hall, London, 1983).
12. S.-J. Im, A. Husakou, and J. Herrmann, "Guiding properties and dispersion control of kagome lattice hollow-core photonic crystal fibers," Opt. Express **17**, 13050–13058 (2009).
13. L. Chen, "Modelling of photonic crystal fibres," Ph.D. thesis, University of Bath (2009).
14. L. Chen and D. M. Bird, "Guidance in Kagome-like photonic crystal fibres II: Perturbation theory for a realistic fibre structure," Submitted to Opt. Express (2011).
15. T. Birks, D. Bird, T. Hedley, J. Pottage, and P. Russell, "Scaling laws and vector effects in bandgap-guiding fibres," Opt. Express **12**, 69–74 (2004).

#141859 - $15.00 USD
Received 27 Jan 2011; accepted 9 Mar 2011; published 25 Mar 2011

16. S. Kawakami, "Analytically solvable model of photonic crystal structures and novel phenomena," J. Lightwave Technol. **20**, 1644–1650 (2002).
17. A. Kumar, A. N. Kaul, and A. K. Ghatak, "Prediction of coupling length in a rectangular-core directional coupler: an accurate analysis," Opt. Lett. **10**, 86–88 (1985).
18. P. S. J. Russell, T. A. Birks, and F. D. Lloyd-Lucas, "Photonic bloch waves and photonic band gaps," in *Confined Electrons and Photons: New Physics and Application*, E. Burstein and C. Weisbuch, eds. (Plenum, New York, 1995), pp. 585–633.
19. G. J. Pearce, T. D. Hedley, and D. M. Bird, "Adaptive curvilinear coordinates in a plane-wave solution of maxwell's equations in photonic crystals," Phys. Rev. B **71**, 195108 (2005).
20. G. Pearce, J. Pottage, D. Bird, P. Roberts, J. Knight, and P. Russell, "Hollow-core pcf for guidance in the mid to far infra-red," Opt. Express **13**, 6937–6946 (2005).
21. J. Pottage, D. Bird, T. Hedley, J. Knight, T. Birks, P. Russell, and P. Roberts, "Robust photonic band gaps for hollow core guidance in pcf made from high index glass," Opt. Express **11**, 2854–2861 (2003).
22. T. A. Birks, G. J. Pearce, and D. M. Bird, "Approximate band structure calculation for photonic bandgap fibres," Opt. Express **14**, 9483–9490 (2006).
23. J. M. Stone, G. J. Pearce, F. Luan, T. A. Birks, J. C. Knight, A. K. George, and D. M. Bird, "An improved photonic bandgap fiber based on an array of rings," Opt. Express **14**, 6291–6296 (2006).
24. N. M. Litchinitser, A. K. Abeeluck, C. Headley, and B. J. Eggleton, "Antiresonant reflecting photonic crystal optical waveguides," Opt. Lett. **27**, 1592–1594 (2002).

1. Introduction

Hollow-core photonic crystal fibres (PCFs) consist of a low-index air hole surrounded by a periodic cladding structure [1]. This periodic dielectric constant generates photonic bandgaps to prevent light spreading outside the central defect. The air-guided light has many applications owing to its low attenuation [2] and nonlinear effects [3, 4].

Recently, a novel class of PCFs has been reported, attracting intense interest. These are hollow-core, with a Kagome or square-lattice cladding [5–7]. The cladding configuration known as the 'Kagome' structure is formed by three parallel groups of glass struts at an angle of $4\pi/3$ to each other, as shown in Fig. 1(a). Figure 1(b) shows a square-lattice hollow-core PCF, whose cladding structure has two sets of orthogonal glass strips. These PCFs have a large pitch, where Λ is typically 12 μm for Kagome PCFs [5] and 15–17 μm for square-lattice PCFs [6]. This makes light guidance possible in the visible optical spectrum. Moreover, they exhibit very wide high-transmission windows, several times broader than for bandgap-guiding hollow-core PCFs [5, 6]. These advantages make them excellent candidates for nonlinear optical effects in gases. For instance, up to 45 coherent Stokes and anti-Stokes lines can be observed with wavelengths spanning from 325 nm to 2300 nm in hydrogen-filled Kagome PCFs [7].

A striking fact of this class of PCFs is that the cladding geometry in both Kagome and square-lattice hollow-core PCFs does not support photonic bandgaps [5–7]. The coexistence of the fundamental mode and cladding modes at the same frequency and propagation constant implies that this guidance cannot be explained by bandgap guidance but is governed by a novel physical mechanism. Previous studies have found that light is confined because of the low density of the cladding modes and the weak interaction between them and the fundamental guided mode [5–7]. Further analysis through a comparison between a typical bandgap-guiding hollow-core PCF and Kagome PCF found that, although the distance between the propagation constants of the strut modes and fundamental mode in bandgap-guiding PCFs is several times larger than that in Kagome PCFs, the overlap of the wavefunctions between these modes in Kagome PCFs is one order of magnitude lower [8]. However, these studies are largely descriptive and qualitative concerning the guidance mechanism; they do not really explain why well-localised modes can exist in the absence of a bandgap and they do not provide a quantitative analysis of the attenuation. A comparison between Kagome PCFs and Bragg fibres consisting of concentric rings of glass indicates that the existence of additional glass struts in the former greatly increases the leakage [9, 10]. However, this still does not fully explain the guidance in Kagome

#141859 - $15.00 USD Received 27 Jan 2011; accepted 9 Mar 2011; published 25 Mar 2011

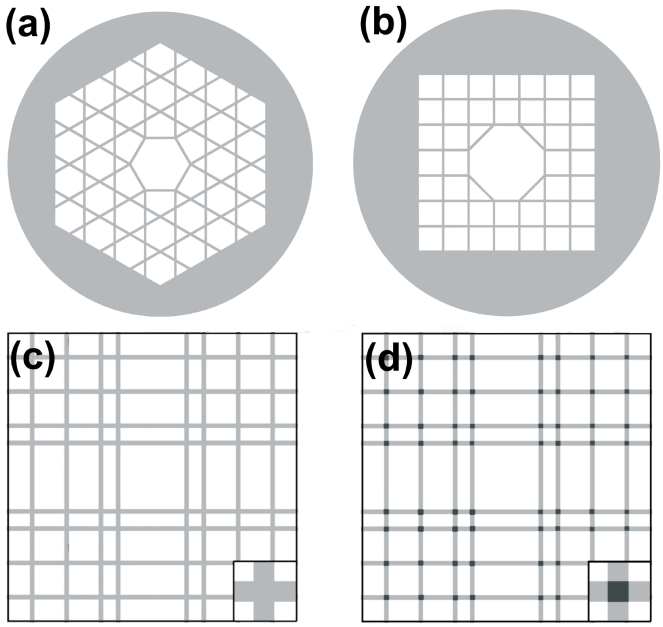

Fig. 1. Schematic of transverse planes of hollow-core PCFs. The cladding structure in (a) is a Kagome lattice, (b) is a square-lattice hollow-core PCF. Corresponding scanning electron micrographs can be found in Refs. [6] and [7]. Rectangular model PCFs are shown in (c) and (d). (c) is a realistic model PCF in which the dielectric constant of the intersections is equal to that of the glass strips, as indicated in the inset. (d) is an ideal model structure for the application of the scalar governing equation; the inset shows that the intersections have a higher dielectric constant than the strips.

PCFs because the guidance mechanisms in these two types of fibres are different.

For a fuller understanding of this novel guidance mechanism, the central question about the origin and magnitude of the leakage should be physically answered. This will help to improve our understanding of the unique features of the guidance and provide a foundation for simplification and optimisation in simulations and fabrication. Analysis of PCFs is made difficult by the relatively complex geometry and the vector nature of the governing equations. In the transverse plane of PCFs, the transverse component of the magnetic field satisfies [11]

$$(\nabla_t^2 + n^2 k_0^2 - \beta^2)\mathbf{h}_t = (\nabla_t \times \mathbf{h}_t) \times \nabla_t \ln n^2, \tag{1}$$

where $k_0 = 2\pi/\lambda$ and λ is the vacuum wavevector, β is the propagation constant, n^2 is the dielectric function which describes the transverse structure of the PCF, and ∇_t is the transverse gradient operator. The vector character of Eq. (1) is contained in the right-hand side. Although numerical tools, such as the finite element method [12] or boundary element method [13], can be used to obtain essentially exact solutions, this does not provide a physical understanding of the nature of the guidance.

In this paper and a following paper [14] we take a new approach to analyse guidance in Kagome-like PCFs. Our aim is first to develop a simplified structure for which analytic solutions can be found. We then use perturbation theory to analyse the difference between our ideal structure and a realistic fibre, which enables us to develop methods for calculating the

#141859 - $15.00 USD Received 27 Jan 2011; accepted 9 Mar 2011; published 25 Mar 2011

attenuation. The first simplification is to consider a scalar governing equation [11]:

$$(\nabla_t^2 + n^2 k_0^2 - \beta^2)\mathbf{h}_t = 0, \tag{2}$$

where the magnetic field $\mathbf{h}_t$ is either x or y polarised in the transverse plane. Although this approximation has a limited quantitative accuracy, it provides a useful insight into a wide range of PCFs [15]. It also makes calculations more efficient. In our case we will solve Eq. (2) for a model structure and include vector terms as a perturbation.

Both Kagome and square-lattice PCFs have sufficiently complicated fibre structures to prevent the governing equation, even in the scalar approximation, from being easily solved. We therefore use a modified square-lattice structure, as shown in Figs. 1(c) and 1(d). The cladding in these structures consists of square air holes surrounded by thin glass strips of uniform thickness, which is similar to the experimentally reported square-lattice PCFs. The main difference is that the central air defect in our models is created by moving the four glass strips enclosing the central air hole by a small distance; the positions of the other glass strips are unchanged. The defect in our model therefore not only covers the central air hole, but also extends along the x and y axes. The two model structures differ only at the intersections of the glass strips. Figure 1(c) shows a structure which, in principle, can be fabricated. However, it still does not allow for a simple solution. We therefore use the structure shown in Fig. 1(d) as our ideal model structure. It differs from Fig. 1(c) in having a higher refractive index at the intersections of the glass strips. The key point is that this design makes the total dielectric function separable into identical sets of parallel glass slabs along the two axes and allows us to obtain analytical solutions. A similar approach has been used in previous work on waveguides [16, 17]. The difference in the structures shown in Figs. 1(c) and 1(d) will also be treated using perturbation theory.

In this paper, guidance in the ideal model structure will be analysed using the scalar governing equation. We derive analytical solutions for the full set of modes. It will be shown that an exponentially localised fundamental mode exists within the central defect even without the existence of photonic bandgaps. This property forms the basis of our analysis of guidance in more realistic Kaogme-like PCF structures. The existence of localised in-plane modes in our model structure has been found in previous work [16]. In this paper, we extend this work to include the full set of out-of-plane modes and to demonstrate that the localised fundamental mode exists over a broad range of frequencies. Importantly, the analytic results also allows us to use perturbation theory to analyse attenuation in a realistic fibre structure, as will be discussed in a following paper [14].

This paper is organised as follows. In Section 2, the application of a transfer matrix method is demonstrated for calculating the cladding and guided modes within a supercell geometry for the idealised model structure. Section 3 presents results based on the analytic method derived in Section 2 and discusses the nature of the modes close to the air-line in terms of being air-guided or glass-guided. The conclusion is given in Section 4.

2. Solution for scalar model structure

2.1. Separation of variables

The model structure presented in Fig. 1(d) has an identical variation of the dielectric constant along both x and y directions in the transverse plane. This feature makes the two-dimensional dielectric function separable as

$$n^2(x,y) = n_a^2 + \triangle n^2(x) + \triangle n^2(y), \tag{3}$$

where n_a^2 is the dielectric constant for the air holes, and the function $\triangle n^2$ gives the difference of the dielectric constant between the glass strips and air holes in each direction. Thus, $\triangle n^2$ takes

#141859 - $15.00 USD Received 27 Jan 2011; accepted 9 Mar 2011; published 25 Mar 2011

the value $n_g^2 - n_a^2$ for the glass regions and zero for the air regions, where n_g^2 is the dielectric constant of glass. The value of the high dielectric constant at the intersections of the glass strips is therefore $2n_g^2 - n_a^2$. Because of this decomposition of the dielectric function, the field $h(x,y)$ in the scalar governing equation can be separated as $h(x,y) = X(x)Y(y)$. Substituting this into Eq. (2) leads to the dimensionless equations

$$\frac{d^2X(x)}{dx^2} + [p_x(x)\Lambda]^2 X(x) = 0, \quad \text{with} \quad [p_x(x)\Lambda]^2 = (k_0\Lambda)^2[n_a^2 + \triangle n^2(x)] - (\beta\Lambda)^2 - \xi \tag{4}$$

and

$$\frac{d^2Y(y)}{dy^2} + [p_y(y)\Lambda]^2 Y(y) = 0, \quad \text{with} \quad [p_y(y)\Lambda]^2 = (k_0\Lambda)^2 \triangle n^2(y) + \xi, \tag{5}$$

where a constant pitch Λ is introduced and ξ acts as a separation constant. The position variables, x and y, are now dimensionless through division by Λ. At the high-index intersections, the magnitude of the normalised transverse wavevector K_g takes the value: $K_g^2 = (p_{xg}\Lambda)^2 + (p_{yg}\Lambda)^2 = (k_0\Lambda)^2(2n_g^2 - n_a^2) - (\beta\Lambda)^2$, where the subscript g represents the values of p_x and p_y in the glass regions. A trigonometric function can thus be introduced to replace ξ and we write separable transverse wavevectors as

$$(p_{xg}\Lambda)^2 = K_g^2 \cos^2\theta \quad \text{and} \quad (p_{yg}\Lambda)^2 = K_g^2 \sin^2\theta, \tag{6}$$

where θ represents the angle relative to the x axis of the transverse wavevector in the high-index intersections. For simplicity a variable $C = \cos(2\theta)$ is used to replace θ. The wavevector components can then be written as

$$(p_{xg}\Lambda)^2 = K_g^2(1+C)/2, \quad (p_{yg}\Lambda)^2 = K_g^2(1-C)/2. \tag{7}$$

The equivalent expressions in the air regions become

$$(p_{xa}\Lambda)^2 = K_g^2(1+C)/2 - (k_0\Lambda)^2\left(n_g^2 - n_a^2\right) \tag{8}$$

and

$$(p_{ya}\Lambda)^2 = K_g^2(1-C)/2 - (k_0\Lambda)^2\left(n_g^2 - n_a^2\right). \tag{9}$$

The scalar governing equation has been separated along two orthogonal directions and the solutions can be parameterised by the variables β and C. By looking at Eq. (7) or Eqs. (8) and (9), the solutions can be sorted into two types: 'symmetric modes' with $C = 0$ and 'non-symmetric modes' with $C \neq 0$. These have the same or different transverse wavevector components in the x and y directions, respectively. The symmetric modes are important because, as we will show later, all the modes of the model structure can be derived from solutions with $C = 0$.

2.2. Matrix expressions for the fields

The separated Eqs. (4) and (5) can be solved analytically. In Ref. [18] field expressions for a one-dimensional periodic dielectric stack have been derived. We now extend this method to a general arrangement of air and glass layers suitable for our model structure.

A schematic of the structure is shown in Fig. 2(a) (see the caption for detail). The solution of Eq. (4) in the N^{th} layer of this structure can be expressed as [18]

$$X_j^N(x) = a_j^N \cos\left[\left(p_{xj}\Lambda\right)\left(x - x_j^N\right)\right] + b_j^N \sin\left[\left(p_{xj}\Lambda\right)\left(x - x_j^N\right)\right] / \left(p_{xj}\Lambda\right), \tag{10}$$

where a_j^N and b_j^N are coefficients which determine the field, $j = a, g$ represents air or glass respectively, and $p_{xj}\Lambda$ is the normalised wavevector component referring to material j. x_j^N denotes a reference point in the N^{th} segment and Λ is chosen as the pitch of the cladding structure.

#141859 - $15.00 USD Received 27 Jan 2011; accepted 9 Mar 2011; published 25 Mar 2011

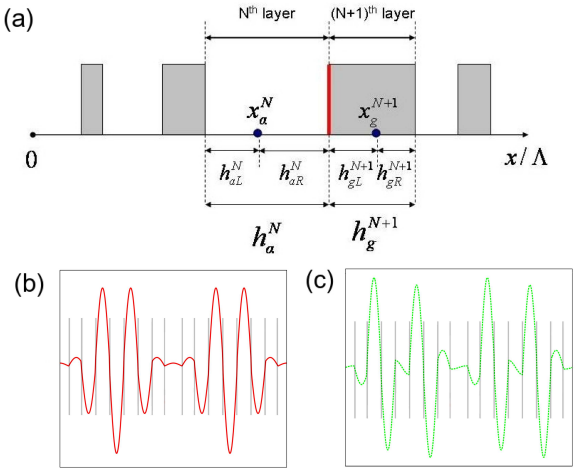

Fig. 2. (a) Sketch of a general one-dimensional arrangement of air and glass regions. The light and dark colours represent air and glass, respectively. The widths of the N^{th} air and $(N+1)^{th}$ glass regions are h_a^N and h_g^{N+1}. Here, x_a^N and x_g^{N+1} are two arbitrary points within the air and glass. All the quantities are made dimensionless through division by Λ. (b) and (c) Examples of even and odd solutions in one dimension of an 8×8 supercell of the model structure.

The expression in Eq. (10) has the advantage of algebraic convenience. The field coefficients, a_j^N and b_j^N, are always real even if β^2 is negative or p_{xj} becomes zero. Moreover, waves in a stop band can also be expressed via real values of a_j^N and b_j^N [18].

At the interface between the N^{th} and $(N+1)^{th}$ layers (shown by the red line in Fig. 2 (a)), both the fields and their derivatives are continuous, leading to the matrix equation

$$\begin{pmatrix} \cos\left[(p_{xa}\Lambda)h_{aR}^N\right] & \sin\left[(p_{xa}\Lambda)h_{aR}^N\right]/(p_{xa}\Lambda) \\ -(p_{xa}\Lambda)\sin\left[(p_{xa}\Lambda)h_{aR}^N\right] & \cos\left[(p_{xa}\Lambda)h_{aR}^N\right] \end{pmatrix}\begin{pmatrix} a_a^N \\ b_a^N \end{pmatrix} = \begin{pmatrix} \cos\left[(p_{xg}\Lambda)h_{gL}^{N+1}\right] & -\sin\left[(p_{xg}\Lambda)h_{gL}^{N+1}\right]/(p_{xg}\Lambda) \\ (p_{xg}\Lambda)\sin\left[(p_{xg}\Lambda)h_{gL}^{N+1}\right] & \cos\left[(p_{xg}\Lambda)h_{gL}^{N+1}\right] \end{pmatrix}\begin{pmatrix} a_g^{N+1} \\ b_g^{N+1} \end{pmatrix}, \tag{11}$$

where the dimensionless parameters h_{aL}^N, h_{aR}^N, h_{gL}^{N+1} and h_{gR}^{N+1} are defined in Fig. 2(a). For simplicity we choose the centre of each layer as the reference point and set $h_{aL}^N = h_{aR}^N = h_j^N/2$. Equation (11) then becomes

$$\underline{a}_g^{N+1} = \underline{\underline{m}}\left(-\frac{h_g^{N+1}}{2}, p_{xg}\Lambda\right)^{-1}\underline{\underline{m}}\left(\frac{h_a^N}{2}, p_{xa}\Lambda\right)\underline{a}_a^N, \tag{12}$$

where

$$\underline{\underline{m}}(h,p) = \begin{pmatrix} \cos(hp) & \sin(hp)/p \\ -p\sin(hp) & \cos(hp) \end{pmatrix} \tag{13}$$

and

$$\underline{a}_j^N = (a_j^N, b_j^N)^T, \qquad \underline{a}_j^{N+1} = (a_j^{N+1}, b_j^{N+1})^T. \tag{14}$$

By using Eq. (12), the field in an arbitrary layer can be expressed in terms of the field in the adjacent layer.

#141859 - $15.00 USD Received 27 Jan 2011; accepted 9 Mar 2011; published 25 Mar 2011

2.3. *Modes in a supercell geometry*

The conversion of the two-dimensional problem into a one-dimensional one makes calculation of the modes in our rectangular model structure very efficient. The transfer matrix method is suitable for a number of geometries, including a perfect cladding, a defect in a cladding or a defect in a supercell geometry. The concept of the 'supercell' is often used in computational solutions [19,20]; each supercell can be viewed as a large unit cell and contains $N \times N$ primitive cells in the transverse plane. In our analysis, we will use a supercell geometry because this leads to a finite number of calculated modes and, most importantly, the modes can be normalised, whether or not they are localised. This will be important in the perturbation analysis in the following paper. We focus only on the modes at the Γ point of the supercell Brillouin zone, which implies that the field coefficients in the centres of neighbouring supercells are the same for each mode. It is expected that the modes at the Γ point can effectively represent all the solutions within a supercell. With an increase of the supercell size, the area of the first Brillouin zone correspondingly decreases. The accuracy of Γ point sampling can be examined through tests of the convergence of solutions with respect to the size of the supercell.

We first restrict our analysis to the symmetric modes with the same transverse wavevector in the x and y directions, i.e. $C = 0$. By choosing the centre of the central defect of a supercell as the origin, the arrangement of the glass layers is symmetric along both axes. Owing to this structural symmetry, the permitted one-dimensional fields have either even or odd symmetry with respect to the centre of the central defect; two examples are shown in Figs. 2(b) and 2(c). To find these two types of modes, a particular value of normalised frequency $k_0\Lambda$ is first chosen. For the symmetric solutions we begin at the origin with the field coefficients $\underline{a} = (1,0)^T$. A trial value of $\beta\Lambda$ is chosen and transfer matrices are used to determine the field at the origin of the next supercell. The $\beta\Lambda$ value is then scanned to determine values for which the field returns to $(1,0)^T$. Similarly, odd modes are found by starting with $\underline{a} = (0,1)^T$. We note that the search for allowed $\beta\Lambda$ values is the only numerical part of the calculation. Once the $\beta\Lambda$ value is determined, the field coefficients are given by analytical expressions. It is also straightforward to normalise the modes, again by using analytical expressions [13].

By using these symmetric modes, the non-symmetric modes with $C \neq 0$ can also be derived. We note that the variables $p_{xg}\Lambda$ and $p_{yg}\Lambda$ serve as the only arguments in Eqs. (4) and (5), respectively. Owing to the identical one-dimensional arrangements of the air and glass regions in both directions, the solutions of these two equations point to the same set of $(p_g\Lambda)^m$ values, where m is a label. If we consider the symmetric modes with $C = 0$, these $(p_g\Lambda)^m$ values are determined only by a set of K_{g0}^m, where K_{g0} is K_g at $C = 0$ and the label m relates to that in $p_g\Lambda$. For a non-symmetric mode with $C \neq 0$, we assume that $p_{xg}\Lambda = (p_g\Lambda)^v$ and $p_{yg}\Lambda = (p_g\Lambda)^u$, where $v \neq u$ because $p_{xg}\Lambda$ and $p_{yg}\Lambda$ are not equal. By using Eq. (7), this non-symmetric mode is related to the symmetric modes v and u by

$$(1+C)K_g^2 = {K_{g0}^v}^2 \tag{15}$$

and

$$(1-C)K_g^2 = {K_{g0}^u}^2. \tag{16}$$

Eqs. (15) and (16) are combined to give

$$K_g^2 = ({K_{g0}^v}^2 + {K_{g0}^u}^2)/2. \tag{17}$$

By substituting expressions for K_g, K_{g0}^u and K_{g0}^v into Eq. (17), the $(\beta\Lambda)^2$ value of this non-symmetric mode is given by

$$(\beta\Lambda)^2 = [(\beta_0^v\Lambda)^2 + (\beta_0^u\Lambda)^2]/2 \tag{18}$$

#141859 - $15.00 USD Received 27 Jan 2011; accepted 9 Mar 2011; published 25 Mar 2011

where β_0^v and β_0^u are propagation constants for the two symmetric modes. After obtaining the propagation constant, the factor C is given by Eq. (15) or (16). This connection indicates that the full set of non-symmetric modes can be obtained from the set of symmetric modes. In practice, we are interested in modes with β close to the air-line. This requires a large range of $(\beta\Lambda)^2$ values for the symmetric modes to be calculated, including those with $(\beta\Lambda)^2$ less than zero. Although solutions when $(\beta\Lambda)^2$ is negative do not exist as propagating modes, they are needed to determine the full set of non-symmetric modes with positive $(\beta\Lambda)^2$.

3. Results in the scalar approximation

3.1. Guidance properties of rectangular hollow-core PCFs

In our simulations, we model a hollow-core PCF using glass strips with a thickness of 0.05Λ, where Λ is the pitch of the perfectly periodic cladding. The refractive indices are 1.0 for the air holes and 1.5 for the glass strips. The central defect is created by moving outward the four glass strips enclosing the central air hole by a distance of 0.125Λ. The arrangement of glass strips in one dimension of an 8×8 supercell is shown in Figs. 2(b) and 2(c).

When considering guidance in PCFs it is useful first to analyse the properties of the perfect periodic cladding structure. This is conveniently done by calculating the photonic density of states (PDOS) [21–23]. The PDOS, as a function of normalised frequency, clearly shows the location of photonic bands and bandgaps. With our rectangular model structure, the method of Section 2 can be extended to calculate the PDOS of the perfect, infinite cladding by using Bloch's theorem. Details of these calculations are given in Ref. [13].

The PDOS is shown in Fig. 3(a), as a function of the normalised frequency $k_0\Lambda$ and the range of normalised propagation constants close to the air-line, i.e. $(\beta - k_0)\Lambda$. The yellow and white regions represent photonic bands and bandgaps, respectively. It is observed that there is a sequence of bandgaps that cross the air-line.

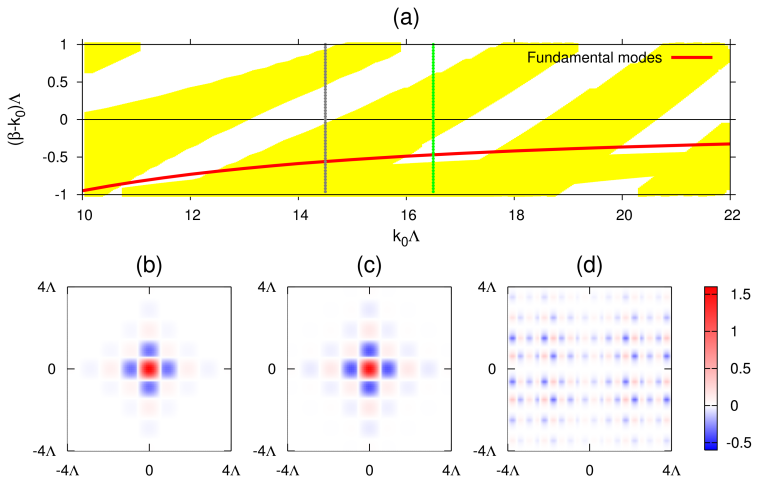

Fig. 3. (a) PDOS and fundamental guided mode for the ideal model PCF structure of Fig. 1(d) and the scalar governing equation. The red line shows the propagation constant of the fundamental mode. The green and black lines are two frequencies for which the field of the modes are plotted in (b) and (c,d), respectively. (b) The fundamental mode with $\beta\Lambda = 16.031$ at $k_0\Lambda = 16.5$. (c) and (d) The fundamental and selected cladding mode with equivalent $\beta\Lambda = 13.941$ at $k_0\Lambda = 14.5$.

We now consider guided modes in the model structure with a central defect. The funda-

#141859 - $15.00 USD Received 27 Jan 2011; accepted 9 Mar 2011; published 25 Mar 2011

mental guided mode is shown by the red line in Fig. 3(a). This has been calculated by using the methodology of Section 2 with a 28×28 supercell. It is not surprising that a guided mode should exist within the bandgaps of the perfect cladding structure; an example of the fundamental mode at $k_0\Lambda = 16.5$ is given in Fig. 3(b). More surprisingly, we find that an exponentially localised mode exists for all normalised frequencies within the given range, whether or not there is a bandgap. An example is given in Fig. 3(c), and Fig. 3(d) shows a cladding state with the same frequency and propagation constant (to within 6 d.p.) as the guided mode in Fig. 3(c). As discussed in the introduction, this coexistence of localised and delocalised modes has been previously noted for our model structure in Ref. [16]. In this paper, a leakage-free mode was found within a continuum of states at a given frequency when investigating photonic waveguides. For our application to PCFs, we note that the exponentially localised fundamental guided mode appears over a wide range of frequencies. There exists a resonant region (which starts in our case at $k_0\Lambda = 56$) where there is no guided mode; this occurs when a new one-dimensional mode is just trapped in the transverse direction across the glass strips [24]. This will be discussed in more detail in a following paper [14] .

Both the coexistence of the fundamental and cladding modes at the same frequency and propagation constant, and the ultra-broad range of guided frequencies have been experimentally observed in Kagome [5, 7] and square-lattice hollow-core [6] PCFs. It is for this reason that we believe that our model PCF structure can provide a useful basis for understanding the guidance mechanism in Kagome and square-lattice hollow-core PCFs.

3.2. Guided modes in the supercell geometry

In order to obtain a set of normalised modes, it is necessary to use a supercell geometry. To demonstrate the nature of the modes we choose an example normalised frequency of $k_0\Lambda = 40$, which lies within a band of cladding states. For convenience, in discussing the modes, we begin with a relatively small 8×8 supercell.

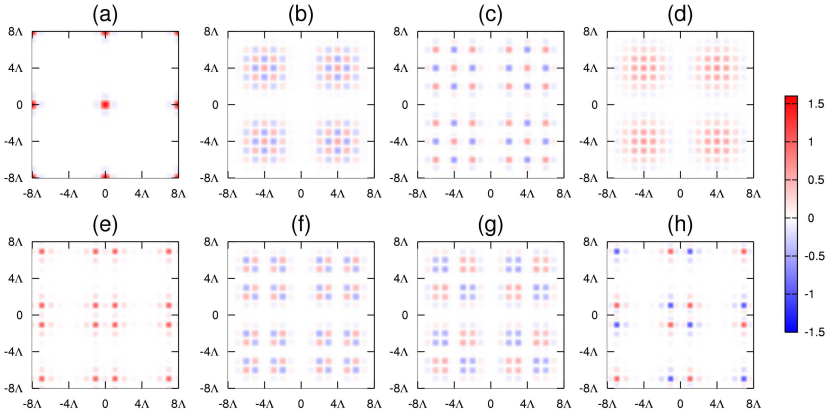

Fig. 4. Field plots in the transverse plane for symmetric modes (i.e. $C = 0$) close to the air-line. The normalised frequency is $k_0\Lambda = 40$, and the $(\beta\Lambda)^2$ values of these modes vary from 1572.73 to 1587.12. The fundamental mode is shown in (a).

We first focus on the symmetric modes which have identical one-dimensional wavefunctions along the x and y directions (i.e. those with $C = 0$). It is convenient to consider these modes as being of three distinct types in terms of their propagation constants. The first is the set of air-guided modes just below the air-line. This set contains eight modes (which is associated with the size of the supercell chosen). These air-guided modes are well separated from other modes

#141859 - $15.00 USD
Received 27 Jan 2011; accepted 9 Mar 2011; published 25 Mar 2011

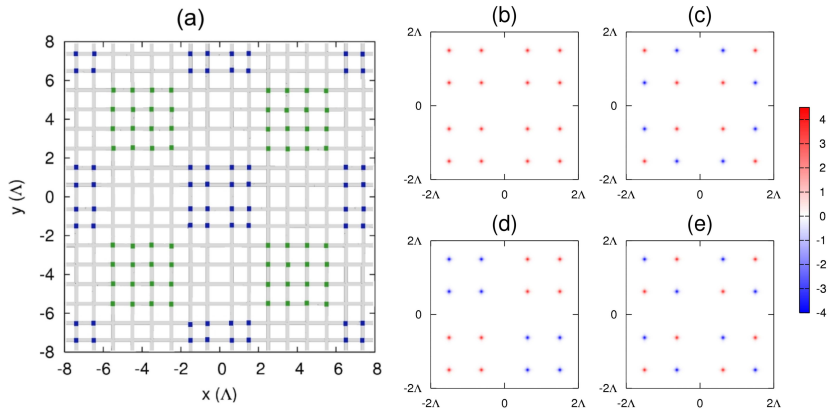

Fig. 5. (a) Schematic diagram of the two regions in which the field is concentrated for high-index modes in an 8×8 supercell. (b-e) Four modes with fields localised in the blue regions in (a). Modes (b) and (c) have even waves in both directions; (d) and (e) have odd waves along the axes. Four other modes have a similar field pattern, but in the green regions of (a).

with lower values of $\beta\Lambda$. The transverse fields of this group of modes nearest to the air-line are shown in Fig. 4; among them is the fundamental guided mode, as shown by Fig. 4(a). The wavefunctions are both even in modes (a) to (e) and both odd in modes (f) to (h) in Fig. 4.

Another group of modes is found with propagation constants well above the air-line. Eight modes are located at $(\beta\Lambda)^2 = 3611.54$, with extremely small differences in the $(\beta\Lambda)^2$ values of less than 10^{-7}. Plots of these modes are shown in Fig. 5, where it can be seen that the fields are located in the high-index intersections of the glass strips. Owing to this property, these modes are referred to as 'high-index modes'.

There are also a large number of solutions with $C = 0$ with $\beta\Lambda$ values much lower than the air-line. Three examples of these modes are shown in Fig. 6. As mentioned above, solutions with negative $(\beta\Lambda)^2$ values are important in determining the full set of non-symmetric modes with positive $(\beta\Lambda)^2$. This also explains why we are interested in the three modes in Fig. 6: they can generate non-symmetric modes with $\beta\Lambda$ values close to the fundamental mode. Figure 6 shows that, unlike the previous two types, the fields of these 'delocalised modes' are no longer confined in a specific region but instead spread throughout the whole transverse plane. Moreover, they exhibit rapid transverse oscillation, as indicated by the alternation of the red and blue colours in these plots.

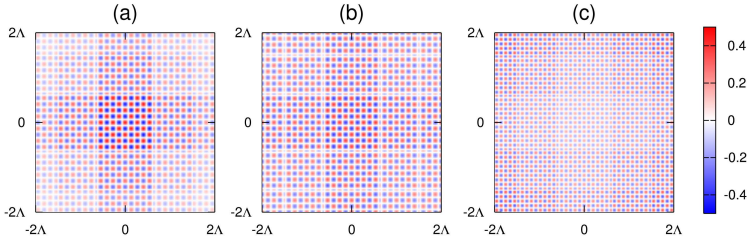

Fig. 6. Example plots of symmetric solutions with delocalised fields. The $(\beta\Lambda)^2$ values are 535.01, 498.25 and -344.78 for (a), (b) and (c), respectively. Note that only the region close to the central defect is shown.

#141859 - $15.00 USD
Received 27 Jan 2011; accepted 9 Mar 2011; published 25 Mar 2011

To form a complete mode map, the non-symmetric modes must also be considered. In principle, every pair of symmetric modes can be combined to give two non-symmetric modes with identical propagation constants but opposite C values. In practice, we are interested only in modes with propagation constants close to the fundamental guided mode. Therefore, there are only two relevant choices of combination of symmetric modes. One is the internal combination of the air-guided modes shown in Fig. 4; the other involves a high-index mode and a delocalised mode, as shown in Figs. 5 and 6, respectively.

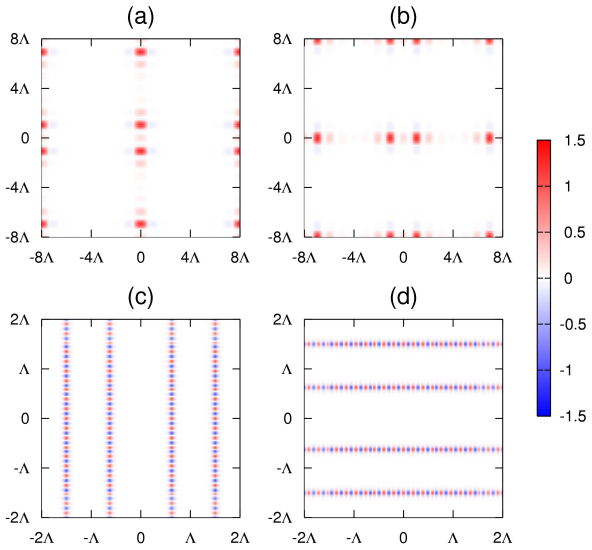

Fig. 7. Two examples of pairs of non-symmetric modes. (a) and (b) Air-guided modes generated by the symmetric modes shown in Figs. 4(a) and 4(e). (c) and (d) Glass-guided modes formed by the combination of the high-index mode of Fig. 5(b) and the delocalised mode of Fig. 6(a). The $(\beta\Lambda)^2$ values are 1579.93 for modes (a) and (b), and 2073.28 for modes (c) and (d).

Figures 7(a) and 7(b) show an example pair of combined air-guided modes, the field patterns of which differ by an angle of $\pi/2$ in the transverse plane because of the opposite C values. The field intensity is still mainly confined in the air holes. Figures 7(c) and 7(d) display examples of the modes formed by a combination of high-index modes and delocalised modes. These modes are glass-guided, and their fields are concentrated along the glass strips. Because of the large number of delocalised modes, these glass-guided modes evenly cover a broad region of $\beta\Lambda$ values and are therefore likely to become very close to the fundamental mode. As observed in Kagome and square-lattice hollow-core PCFs [6, 7], the glass-guided modes are characterised by dramatic oscillation of the spatial fields. Owing to the obvious mismatch of spatial frequencies between the fundamental mode and the glass-guided modes, it can be supposed that there is a suppressed coupling between the two. The leakage caused by the glass-guided modes is therefore expected to be relatively small. This point will be analysed further in a following paper [14].

4. Conclusion

Transfer matrix methods have been developed for an idealised rectangular hollow-core PCF. Within the scalar approximation, a complete set of modes can be calculated within a supercell

#141859 - $15.00 USD Received 27 Jan 2011; accepted 9 Mar 2011; published 25 Mar 2011

geometry. For modes near the air-line there is a clear discrimination into air-guided and glass-guided modes. The existence of an exponentially localised fundamental mode with the same propagation constant as cladding states shows that the model hollow-core PCF can be identified as a prototype of the PCF family that governs light via the weak interaction of modes. This analysis will be extended in a following paper where perturbation theory is used to consider the effects of vector terms in the governing equation and the unrealistic high-index intersections of the idealised model structure.

Acknowledgments

We thank Fetah Benabid and John Roberts for helpful discussions in the course of this work.

#141859 - $15.00 USD Received 27 Jan 2011; accepted 9 Mar 2011; published 25 Mar 2011